2

Basic imaging

2.1 Fourier inversion

A more detailed understanding of the integral defining the coherent flux in Equation (1.39) can be derived by recognising it as a two-dimensional *Fourier transform*, about which there is a well-developed mathematical infrastructure. A brief introduction to the most important properties of the Fourier transform is given in Appendix A.

The Fourier transform can be used to represent any arbitrary (within reason) function f as the sum of a set of sinusoids of different frequencies; for a two-dimensional function $f(\boldsymbol{x})$ this sum can be written as an integral

$$f(\boldsymbol{x}) = \iint_{-\infty}^{\infty} g(\boldsymbol{s}) e^{2\pi i \boldsymbol{s}\cdot\boldsymbol{x}}\, ds_x\, ds_y, \tag{2.1}$$

where $\boldsymbol{x} = (x, y)$ is a two-dimensional spatial coordinate and $\boldsymbol{s} = (s_x, s_y)$ is a two-dimensional *spatial frequency*. The complex sinusoid $e^{2\pi i \boldsymbol{s}\cdot\boldsymbol{x}}$ is a two-dimensional function whose value is constant along lines perpendicular to the vector $\boldsymbol{s}$ and repeats over a distance $1/|\boldsymbol{s}|$ and so Equation (2.1) is equivalent to saying that a function can be composed by summing a set of sinusoidal 'waves' of different wavelengths and orientations.

Given a function $f(\boldsymbol{x})$, the coefficients $g(\boldsymbol{s})$ can be derived using

$$g(\boldsymbol{s}) = \iint_{-\infty}^{\infty} f(\boldsymbol{x}) e^{-2\pi i \boldsymbol{s}\cdot\boldsymbol{x}}\, dx\, dy. \tag{2.2}$$

The process of deriving the coefficient for each spatial frequency is called the Fourier transform and is denoted by the operator $\mathcal{F}$ so that Equation (2.2) is equivalent to writing $g(\boldsymbol{s}) = \mathcal{F}\left[f(\boldsymbol{x})\right]$ and Equation (2.1) is an *inverse Fourier transform* equivalent to writing $f(\boldsymbol{x}) = \mathcal{F}^{-1}\left[g(\boldsymbol{s})\right]$.

With this in mind, Equation (1.39) can be written as

$$F(\boldsymbol{u}) = \mathcal{F}\left[I(\boldsymbol{\sigma})\right], \tag{2.3}$$

where $\boldsymbol{u}$ and $\boldsymbol{\sigma}$ take the places of $\boldsymbol{s}$ and $\boldsymbol{x}$ respectively. Thus if we have measured $F(\boldsymbol{u})$ we can derive $I(\boldsymbol{\sigma})$ using

$$I(\boldsymbol{\sigma}) = \mathcal{F}^{-1}\left[F(\boldsymbol{u})\right]. \tag{2.4}$$

This can straightforwardly be evaluated by computer (and indeed one of the first uses of computers was to evaluate Fourier transforms of data from radio interferometers).

This, then, is the premise of imaging interferometry: the amplitude and phase of the fringe pattern formed by combining the light from two telescopes correspond to the amplitude and phase of a single Fourier component of the angular structure of the object being observed. This component is at a spatial frequency set by the projected baseline $\boldsymbol{u}$. By changing the vector separation of the telescopes one can sample $F(\boldsymbol{u})$ at different values of $\boldsymbol{u}$. With sufficient samples of $F(\boldsymbol{u})$, an image $I(\boldsymbol{\sigma})$ of the object under study can be reconstructed using an inverse Fourier transform.

The definition of 'sufficient samples' is the key question, as Equation (2.1) implies that an infinite number of samples is required in theory. This question will be answered in this chapter in three ways. First, an intuitive idea of the kind of information present at different locations in the (u, v) plane will be obtained by looking at the visibility functions of a number of representative objects. Second, strategies for sampling the (u, v) plane will be explored; and finally, an idea of the effects of limited sampling in certain special cases will be obtained, leading to the idea of 'aperture synthesis'.

In all cases, the interferometer will be assumed to be 'phase stable', in other words the measured fringe phase accurately reflects the object coherent phase. This is an adequate model for some radio interferometers, but in Chapter 3 it will be shown that most optical interferometers show strong phase instabilities due to the Earth's atmosphere. Nevertheless, understanding the properties of interferometric imaging under phase-stable conditions can serve as a good basis for understanding the principles of image reconstruction. More details of the processes of image reconstruction in phase-unstable conditions are presented in Chapter 9.

2.2 Visibility functions of simple objects

Before going on to understand in more detail how well images can be reconstructed from interferometric measurements, it is worthwhile examining the characteristics of the visibility for some simple objects so as to get an intuitive 'feel' for the kind of information about an object which is captured by

this observable, since the Fourier nature of interferometry is initially quite un-intuitive.

2.2.1 Point source

The simplest object that can be observed is a single point-like source of light, for example a star whose diameter is much smaller than the angular resolution of the interferometer. The properties of a fringe pattern for a point source were derived earlier, but redoing the calculation using the Fourier transform provides an introduction to using the Fourier formalism and interpreting the results.

A point-like object can be represented by a Dirac delta function (delta functions represent impulse-like distributions confined to a single point; their properties are described further in Appendix A):

$$I(\boldsymbol{\sigma}) \propto \delta(\boldsymbol{\sigma} - \boldsymbol{\sigma}_0), \tag{2.5}$$

where σ_0 is the angular coordinate of the source. The Fourier transform of a delta function is a complex exponential, so that

$$F(\boldsymbol{u}) \propto e^{2\pi i \boldsymbol{u}\cdot\boldsymbol{\sigma}_0}, \tag{2.6}$$

and normalising we get

$$V(\boldsymbol{u}) = e^{2\pi i \boldsymbol{u}\cdot\boldsymbol{\sigma}_0}. \tag{2.7}$$

Thus $|V(u, v)| = 1$, in other words the fringe contrast when observing a point source is independent of the length or orientation of the baseline.

2.2.2 Binary star system

The linearity of the Fourier transform means that the coherent flux of the fringe pattern observed for a pair of stars will be the sum of the coherent fluxes for each star observed separately. If both stars are unresolved, and one star with flux F_a is at the phase centre and the second star with flux F_b is at an angular offset of σ_0, then the total coherent flux will be given by

$$F(\boldsymbol{u}) = F_a + F_b e^{2\pi i \sigma_0 \cdot \boldsymbol{u}}. \tag{2.8}$$

The coherent flux can be represented in an Argand diagram as the sum of two vectors as shown in Figure 2.1. The vector of length F_a stays fixed along the real axis while the vector of length F_b rotates in the complex plane as the (u, v) coordinate changes, and so the length of the summed vector will go from $F_a + F_b$ at a maximum to $F_a - F_b$ at a minimum (assuming that $F_a > F_b$).

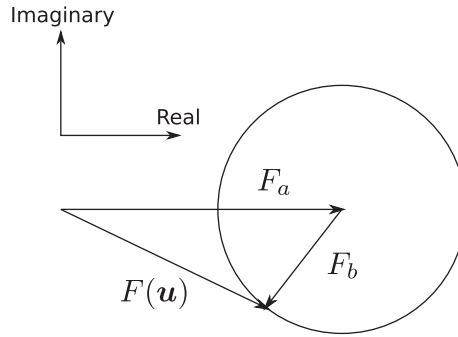

Figure 2.1 Vector sum representation of the coherent flux $F(\boldsymbol{u})$ of a binary system composed of two point sources of flux F_a and F_b.

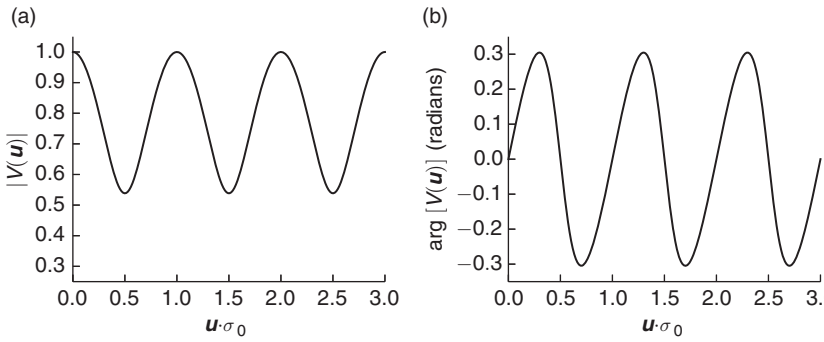

Figure 2.2 Visibility modulus (a) and phase (b) of a binary star with vector separation $\boldsymbol{\sigma}_0$ as a function of the normalised projected baseline $\boldsymbol{\sigma}_0 \cdot \boldsymbol{u}$. The flux of the secondary star is 30% of that of the primary star.

The visibility modulus will therefore oscillate between the values of 1 and $(F_a - F_b)/(F_a + F_b)$. The maximum phase excursion will occur when the summed vector is a tangent to the circular locus of the vector of length F_b, giving a maximum phase value of $\arcsin(F_b/F_a)$. The resulting modulus and phase excursions are shown in Figure 2.2.

2.2.3 Uniform disc

A first-order model for the brightness distribution from a nearby star would be a uniform disc a few milliarcseconds across. We can write the brightness distribution for this disc as

$$I(\boldsymbol{\sigma}) \propto \mathrm{rect}(|\boldsymbol{\sigma}|/\theta_d), \tag{2.9}$$

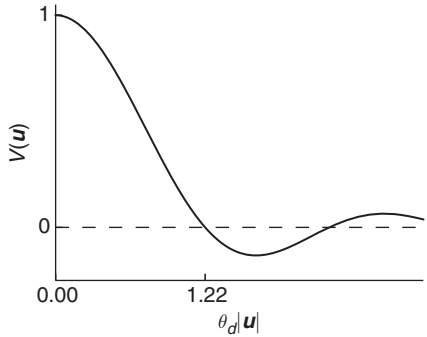

Figure 2.3 Visibility of a point source of a uniform disc such as a star. For a star at the phase centre the visibility is purely real.

where rect is the unit rectangular top-hat function given in Equation (1.59) and θ_d is the angular diameter of the star. The visibility function is given by the normalised Fourier transform

$$V(\boldsymbol{u}) = 2\text{jinc}(\pi\theta_d|\boldsymbol{u}|), \tag{2.10}$$

where the jinc function is defined as

$$\text{jinc}(x) \equiv \frac{J_1(x)}{x} \tag{2.11}$$

and where J_1 is the order-1 Bessel function of the first kind. The jinc function, sometimes known as the Besinc function, is like the well-known sinc function (defined in Equation (1.61)), which is the Fourier transform of a one-dimensional top-hat function. The square of the jinc function describes the intensity distribution of the Airy disc pattern, which we met when considering the resolution of a circular telescope.

The visibility function is real everywhere and circularly symmetric in the (u, v) plane and is plotted in Figure 2.3. The visibility modulus generally decreases with increasing projected baseline and goes through a null for $|\boldsymbol{u}| = 1.22/\theta_d$, in other words for a projected baseline length of $1.22\lambda/\theta_d$. Note that the null in visibility does not mean that the measured *intensity* goes to zero: it means that the contrast of the fringes goes to zero so that the fringes disappear and so the fringe pattern becomes a uniformly illuminated field.

Michelson and Pease (1921) used the position of this null in the visibility in their experiment to measure the angular diameter of Betelgeuse. They used a pair of mirrors mounted on a steel beam as 'outriggers' to the Mt Wilson 100-inch (2.5-m) telescope to form the two apertures of the interferometer and observed the fringes seen for different separations of the mirrors.

Noting the mirror separation at which the fringes disappeared gave a measurement of the diameter using $\theta_d = 1.22\lambda/B_{\text{null}}$ where B_{null} is the separation of the mirrors when the fringes dissapeared. Betelgeuse has one of the largest apparent diameters of any star at about 40 mas, so that at a visible wavelength of 500 nm the fringes should disappear when the mirror separation is about 3.1 m, approximately the distance observed in the experiment.

A star like the Sun at a distance of 10 parsecs will appear to be about 0.8 milliarcseconds in diameter and the fringes will disappear for baselines of about 700 m when observing at a near-infrared wavelength of 2.2 μm. If the maximum telescope separation available is only $B_{\text{max}} = 100$ m then the fringe visibility modulus will always be greater than 99%. We can say that stars of size $\theta_d \ll \lambda/B_{\text{max}}$ are 'unresolved'.

2.2.4 Gaussian disc

A uniform disc model is a relatively accurate representation for solar-type stars, but many evolved stars such as Mira variables have extended atmospheres meaning that the edge of the stellar disk is more 'fluffy'. Various limb-darkening models can be used to describe such stars but a simple model of an extreme limb-darkening profile is a two-dimensional Gaussian intensity distribution:

$$I(\boldsymbol{\sigma}) \propto e^{-4\ln 2|\boldsymbol{\sigma}|^2/\theta_d^2}, \tag{2.12}$$

where θ_d is the full width at half maximum (FWHM) of the Gaussian. The Fourier transform of a Gaussian is also a Gaussian; the visibility function is given by

$$V(\boldsymbol{u}) = e^{-4\ln 2|\boldsymbol{u}|^2/\rho_d^2}, \tag{2.13}$$

where $\rho_d = 0.883/\theta_d$ is the FWHM of the visibility curve. The visibility curve is shown in Figure 2.4.

2.2.5 Objects offset from the phase centre

An important set of properties of the Fourier transform, which is useful in deriving visibility functions, are a consequence of the *convolution theorem*. For any two functions $f(\boldsymbol{x})$ and $g(\boldsymbol{x})$ with Fourier transforms of and $F(\boldsymbol{s})$ and $G(\boldsymbol{s})$, respectively, the convolution theorem states that

$$\mathcal{F}\{fg\} = F * G \tag{2.14}$$

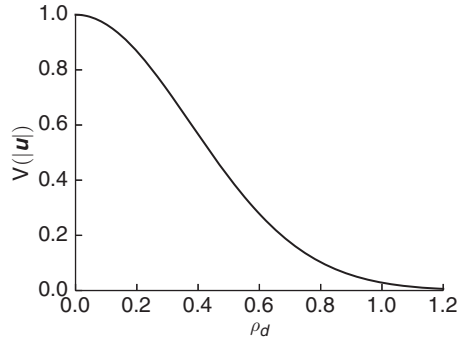

Figure 2.4 Visibility function for a Gaussian disc.

and

$$\mathcal{F}\{f * g\} = FG, \tag{2.15}$$

where $*$ denotes the convolution.

The convolution of two two-dimensional functions $f_1(\boldsymbol{x})$ and $f_2(\boldsymbol{x})$ is defined as

$$(f_1 * f_2)(\boldsymbol{x}) \equiv \iint_{\text{All space}} f_1(\boldsymbol{x}')f_2(\boldsymbol{x} - \boldsymbol{x}')\, dA, \tag{2.16}$$

where dA is an element of area. The ideas surrounding convolution are explained in Appendix A, but the simplest useful property of convolution comes from convolution with a Dirac delta function: convolving any function with a delta function offset from the origin by an amount $\boldsymbol{x}_0$ has the effect of shifting the function by x_0, i. e.,

$$f(\boldsymbol{x}) * \delta(\boldsymbol{x} - \boldsymbol{x}_0) = f(\boldsymbol{x} - \boldsymbol{x}_0). \tag{2.17}$$

This result, together with the convolution theorem, can be used, for example, to compute the visibility function of a star which is offset from the phase centre by some amount $\boldsymbol{\sigma}_0$. We write the brightness distribution of the star as

$$I(\boldsymbol{\sigma}) \propto \text{rect}(|\boldsymbol{\sigma}|/\theta_d) * \delta(\boldsymbol{\sigma} - \boldsymbol{\sigma}_0) \tag{2.18}$$

so the convolution theorem means that the visibility function is the product of the visibility functions of the centred disc and the offset delta function:

$$V(\boldsymbol{u}) = \frac{2J_1(\theta_d|\boldsymbol{u}|)}{\theta_d|\boldsymbol{u}|} e^{2\pi i \boldsymbol{u}\cdot\boldsymbol{\sigma}_0}. \tag{2.19}$$

It can be seen from the above expression that the phase of the visibility carries the information about the position of the object with respect to the phase centre, while the modulus carries the information about the size of the object.

2.2.6 Rules of thumb

The above examples display a number of properties typical of visibility functions:

- The visibility at the origin of the (u, v) plane is always unity and the visibility modulus has equal or lower values elsewhere. This is a general property arising from the definition of visibility and the fact that the object brightness distributions are non-negative.
- The smaller the object, the larger the baseline length required to see significant deviations of the visibility from unity: the characteristic baseline length to see these deviations is of the order of λ/θ where θ is a characteristic angular scale for the object. The reciprocal relationship between the baseline length and angular scale arises from the *scaling* property of Fourier transforms (see Appendix A) and is linked to the use of the term 'reciprocal space' to describe the result of a Fourier transform.
- Smoother brightness distributions like the Gaussian have a lower visibility modulus on long baselines than sharper functions like the uniform disc or the binary. This can be thought of as sharp features in the object corresponding to high-frequency structure, and high frequencies are measured on long baselines.
- Brightness distributions such as the uniform disc and the Gaussian, which are symmetric about the phase centre, have visibility functions which are purely real, i. e. the phase is either 0° or 180° for all $\boldsymbol{u}$. This is a general property of the Fourier transforms of real point-symmetric functions (i. e. functions $f(\boldsymbol{\sigma})$ whose values are real everywhere and for which $f(\boldsymbol{\sigma}) = f(-\boldsymbol{\sigma})$ everywhere).
- All the visibility functions have the property of *Hermitian symmetry* in that $V(\boldsymbol{u}) = V^*(-\boldsymbol{u})$, where the star denotes taking the complex conjugate. This is a general property of the Fourier transforms of real functions, but can also be thought of as arising from the fact that the same pair of telescopes p and q can be equally well used to give baselines of $\boldsymbol{B}_{pq}$ or $\boldsymbol{B}_{qp} = -\boldsymbol{B}_{pq}$, the only difference being that, when the roles of the two telescopes are interchanged, the direction of fringe displacement denoted as a positive change of phase needs to be reversed.

As can be seen, these properties of the visibility arise from the properties of the Fourier transform itself. Other important properties of the Fourier transform are summarised in the Appendix A and are mentioned as they arise in the text.

2.3 Sampling the Fourier plane

The coherent flux of the fringes seen in an interferometer consisting of a pair of telescopes provides a sample of the coherent flux at a single location $\boldsymbol{u}_{ij}$ in the (u, v) plane. The number of samples of the coherent flux, in other words the (u, v)-plane coverage, can be increased in a number of ways.

2.3.1 Moving telescopes

The most obvious way to do this is to change the baseline by moving one or both of the telescopes. This was possible to do in the space of a few minutes with the Interféromètre à Z Télescopes (I2T) (Koechlin, 1988) because the telescopes were mounted on rails and had a minimal beam relay system – the beam paths were in open air.

In modern interferometers the beam-relay system is more complex and can take hours to realign. As a result the process of moving a single telescope can take many hours and so baseline reconfiguration is usually done during the day.

2.3.2 Telescope arrays

A faster way to increase the number of samples is to use more than two telescopes and to measure fringes on all the baselines between them. For a set of M telescopes, there are $\frac{1}{2}M(M-1)$ pairs and so in principle this number of (u, v) points can be sampled simultaneously.

Some care has to go into the placement of the telescopes in order to maximise the sampling. Particularly regular spacings of telescopes such as that shown in Figure 2.5(a) have the same baseline repeated a number of times in the array, and so the set of four telescopes allows the sampling of only three distinct baselines instead of six. Such an arrangement is known as a 'redundant' array (lower part of Figure 2.5(b)), while a telescope arrangment such as that shown above in Figure 2.5(b) is called 'non-redundant' and samples six distinct baselines.

Redundancy is less of a problem in two-dimensional array layouts. Figure 2.6 shows one of the layouts of the telescopes in the Magdalena Ridge Observatory interferometer and the corresponding set of baselines. Although this layout has a regular structure and contains repeated baselines, the overall number of distinct baselines is 36, which is 80% of the 45 baselines possible for a completely non-redundant array.

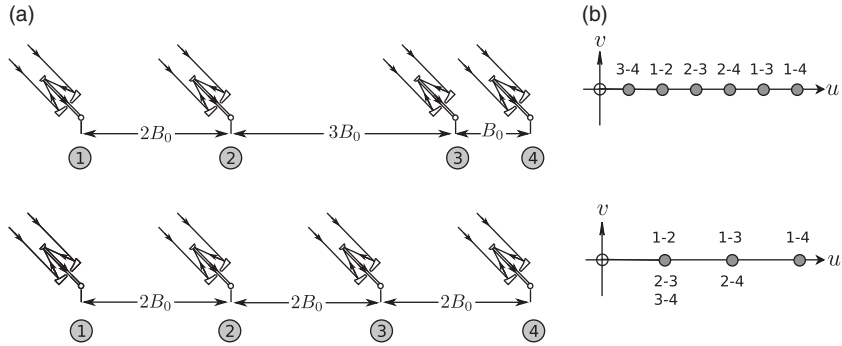

Figure 2.5 Telescopes arranged in different one-dimensional configurations (a) and the corresponding baseline sampling, labeled with the telescope pairs that sample that baseline (b). The lower configuration is termed redundant because at least one baseline is repeated, and as a result fewer distinct (u, v) points are sampled.

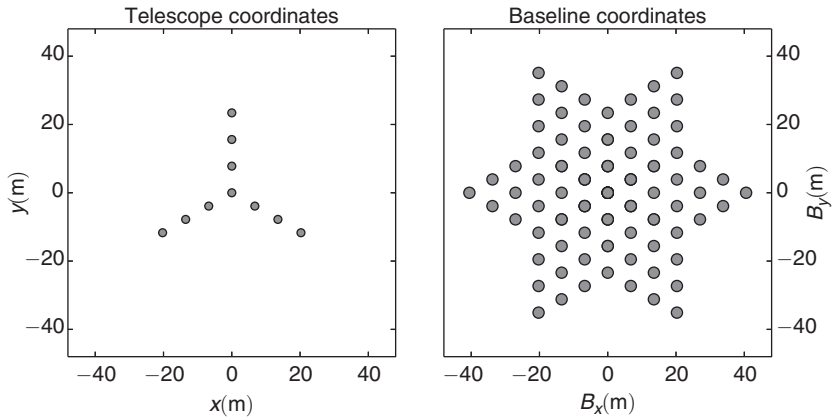

Figure 2.6 A telescope layout for the Magdalena Ridge Observatory interferometer (a) and the resulting baseline coverage (b).

2.3.3 Earth-rotation synthesis

The (u, v) coverage obtainable with a given set of telescopes can be increased by making use of Earth rotation. All ground-based interferometers are sited on a turntable that rotates by 360° once per day – the Earth. Since the (u, v) plane is fixed with respect to a coordinate system based on the direction of the object under study, the projection of the baseline between a pair of telescopes which are stationary on the Earth's surface has different projections onto the

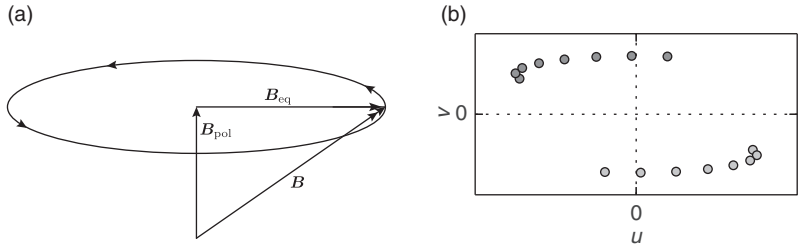

Figure 2.7 The baseline vector $\boldsymbol{B}$ rotating about the Earth's axis (a) and the corresponding (u, v) coverage for an 8-hour track for the observation of an example source (b). The (u, v) coverage is shown with one observation per hour of track. Each observation gives two (u, v) samples due to the Hermitian symmetry of the Fourier transform.

(u, v) plane if observations are made at different times of night as the object rises and sets in the sky.

The effect of Earth rotation is easiest to see for an object at the celestial pole (for example the star Polaris) and an east–west baseline, i. e. one parallel to the equatorial plane of the Earth. In this case the baseline vector describes a circle over the course of 24 hours as seen from the vantage point of the star. Every fringe observation on a given baseline $\boldsymbol{B}_{ij}$ also serves to provide the value of the symmetric baseline $\boldsymbol{B}_{ji}$, so a set of observations made over a 12-hour period suffice to measure the object visibility function over the complete circumference of a circle in the (u, v) plane.

A more general geometry is shown in Figure 2.7, where the object is not sited at the celestial pole and the baseline vector $\boldsymbol{B}$ has a finite polar component $\boldsymbol{B}_{\text{pol}}$ as well as an equatorial component $\boldsymbol{B}_{\text{eq}}$. As the Earth rotates, the polar component remains fixed in space while the equatorial component describes a circle. Seen from the vantage point of a star, the circle is projected on to an ellipse, leading to the baseline describing an ellipse in the (u, v) plane. As shown in Figure 2.7, the centre of the ellipse is offset from the origin of the (u, v) plane by an amount which depends on the projection of $\boldsymbol{B}_{\text{pol}}$ onto the plane perpendicular to the line-of-sight to the star.

The combination of using multiple telescopes and Earth-rotation synthesis can lead to good sampling of the (u, v) plane as shown in Figure 2.8.

2.3.4 Wavelength synthesis

If a pair of telescopes is used to make interference fringe observations at a number of different wavelengths, then the (u, v) point sampled at each wavelength will be different as the (u, v) point depends on the ratio of the baseline

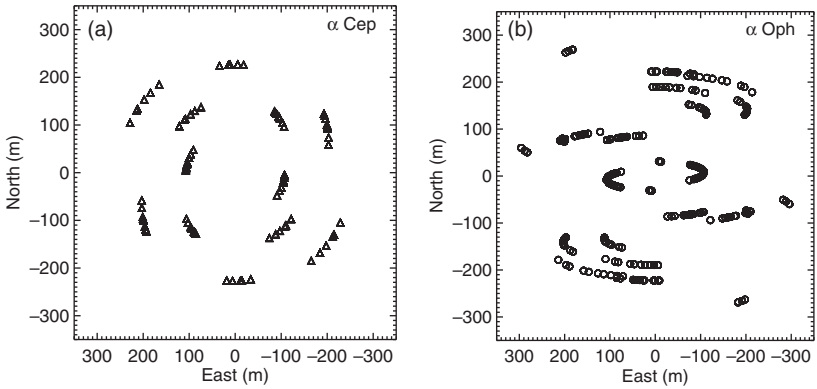

Figure 2.8 Earth-rotation synthesis tracks for the CHARA telescope array observations of two different stars, from Zhao *et al.* (2009). The star α Cephei is relatively close to the celestial pole (declination $\approx 63°$) and so the (u, v) tracks are more circular while α Ophiuchi is nearer to the celestial equator (declination $\approx 13°$) and so the (u, v) tracks are more elongated.

to the wavelength. This can be used to increase the (u, v) sampling of a given set of observations. However, the interpretation of these 'wavelength-synthesis' observations needs to be tempered with caution as they are only easy to interpret if the object shape can be assumed to be the same at all the wavelengths measured. This may be a reasonable constraint if the wavelength range used is small but becomes less valid as the wavelength range increases.

The (u, v) coverage offered by wavelength synthesis consists of a number of scaled copies of the (u, v) coverage available at a single wavelength. Thus the (u, v) coverage will consist of radial streaks as shown in Figure 2.9.

2.4 The image-plane effects of Fourier-plane sampling

2.4.1 The synthesised image

Equation (2.4) shows that it is possible in principle to reconstruct the object brightness distribution exactly if we measure the coherent flux $F(\boldsymbol{u})$ for all values of $\boldsymbol{u}$. In practice we can only measure $F(\boldsymbol{u})$ for at a finite set of discrete values of $\boldsymbol{u}$ rather than completely covering the (u, v) plane.

The effects of this finite sampling can be understood by studying the synthesised image, in other words the image that comes from inverse Fourier

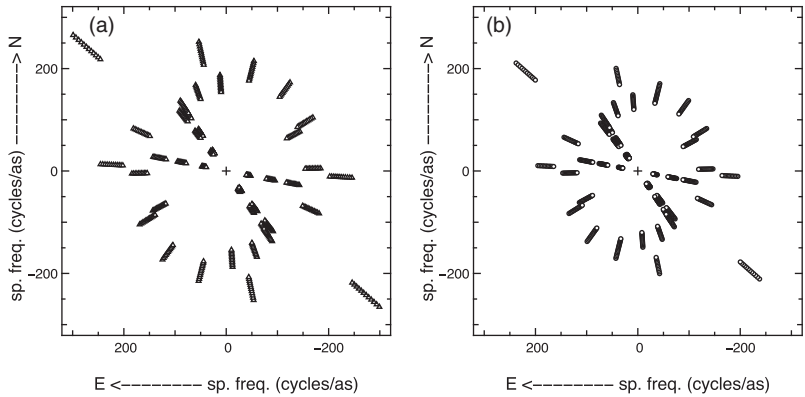

Figure 2.9 Wavelength-synthesis (u, v) coverage of VLTI observations of the star HD87643 in the astronomical H (a) and K (b) bands (from Millour *et al.*, 2009). The radial lines are due to the different spatial frequencies observed on the same baseline at different wavelengths within these bands. Note that the (u, v) coordinates are denoted in units of cycles per arcsecond, a common convention in optical interferometry.

transforming the sampled coherent flux data, and comparing it to the object which produced the data.

For an object brightness distribution given by $I(\boldsymbol{\sigma})$ and corresponding coherent flux $F(\boldsymbol{u}) = \mathcal{F}[I(\boldsymbol{\sigma})]$, the sampled coherent flux $\hat{F}$ can be represented by multiplying the true coherent flux by a sampling function consisting of a set of delta functions:

$$\hat{F}(\boldsymbol{u}) = F(\boldsymbol{u}) \sum_k \delta(\boldsymbol{u} - \boldsymbol{u}_k), \tag{2.20}$$

where $\{\boldsymbol{u}_k\}$ is the set of sample locations in the (u, v) plane. A 'synthesised image' (sometimes called the 'dirty image') $\hat{I}(\boldsymbol{\sigma})$ can be reconstructed by taking the inverse Fourier transform of the sampled data. The convolution theorem can be used to show that

$$\begin{aligned} \hat{I}(\sigma) &= \mathcal{F}^{-1}\left[\hat{F}(\boldsymbol{u})\right] \\ &= I(\boldsymbol{\sigma}) * b(\boldsymbol{\sigma}), \end{aligned} \tag{2.21}$$

where

$$b(\boldsymbol{\sigma}) = \mathcal{F}^{-1}\left[\sum_k \delta(\boldsymbol{u} - \boldsymbol{u}_k)\right]. \tag{2.22}$$

Thus, the effect of making an interferometric image with a given sampling pattern can be described in terms of convolving the object brightness distribution

with a 'point-spread function' $b(\boldsymbol{\sigma})$, which is known in radio astronomy as the 'synthesised beam' or the 'dirty beam'.

The shape of the synthesised beam depends on the details of the (u, v) coverage given by $\{\boldsymbol{u}_k\}$. In general, the angular resolution and field of view of the image will be degraded in comparison with complete coverage of the (u, v) plane, as detailed in the following sections. It is possible to ameliorate some of these degradations by using a process known as 'deconvolution' (discussed in Chapter 9) but the effects of convolution with the synthesised beam can never fully be undone, and so the limitations of the image quality described below give a qualitative idea of the information which is lost as a result of incomplete (u, v) sampling.

2.4.2 Angular resolution

First, we consider an interferometer where the maximum spacing of the telescopes is limited to some value $|\boldsymbol{B}| < B_{\max} = \lambda u_{\max}$, but the coherent flux has been measured at all spacings less than this. The effect of the incomplete information about $F(\boldsymbol{u})$ at larger spacings can be modelled by setting the estimated value to zero outside the region where it is known, i. e.

$$\hat{F}(\boldsymbol{u}) = \mathrm{rect}\left(\frac{|\boldsymbol{u}|}{2u_{\max}}\right) F(\boldsymbol{u}), \tag{2.23}$$

where $\hat{F}$ is the estimate of $F(\boldsymbol{u})$ and the rect function is defined in Equation (1.59). From the convolution theorem (Equation (2.14)) the synthesised image $\hat{I}$ reconstructed by inverse Fourier transforming $\hat{F}$ would then be

$$\hat{I}(\boldsymbol{\sigma}) = I(\boldsymbol{\sigma}) * \mathrm{jinc}(2\pi|\boldsymbol{\sigma}|u_{\max}). \tag{2.24}$$

Thus, the reconstructed image is a convolution of the true image with a jinc function whose angular width (measured from the peak to the first null) is given by

$$\Delta\theta = 1.22/(2u_{\max}) = 1.22\lambda/(2B_{\max}). \tag{2.25}$$

The effect of this convolution is to 'blur out' detail in the image on angular scales of order $\Delta\theta$ and hence to degrade the angular resolution. If the object consists of a pair of stars with separation $\Delta\theta$, then the reconstructed image will consist of a pair of jinc functions, where the peak of one overlaps the null of the other. According to the Rayleigh criterion, this pair is the closest pair that can just be resolved, and so the angular resolution of the image is given by $1.22\lambda/(2B_{\max})$. Comparing this value with that in Equation (1.1) shows that the angular resolution of an interferometer with maximum baseline $B_{\max}$ is

the same as that of a single telescope with diameter $2B_{\max}$. This gives rise to the term 'aperture synthesis': interferometric measurements can be combined to reconstruct images with angular resolutions comparable to that of a telescope with an aperture of size $2B$, without an aperture of such a size being present.

2.4.3 Field of view

The effect of finite sampling density can be modelled assuming that $F(\boldsymbol{u})$ is sampled on a regular square grid of points in the (u, v) plane with spacing Δu. The measurements can be represented by

$$\hat{F}(\boldsymbol{u}) = F(\boldsymbol{u}) \sum_{p=-\infty}^{\infty} \sum_{q=-\infty}^{\infty} \delta(u - p\Delta u, v - q\Delta u), \tag{2.26}$$

with the array of delta functions representing the two-dimensional sampling 'lattice' (note that a lattice is just a two-dimensional version of the Dirac comb function whose Fourier transform is given in Appendix A). The reconstructed image will therefore be a convolution of the true image and the Fourier transform of the lattice, which is a 'reciprocal lattice' with spacing $\Delta\sigma = (\Delta u)^{-1}$, i. e.,

$$\hat{I}(\boldsymbol{\sigma}) = I(\boldsymbol{\sigma}) * \sum_{p=-\infty}^{\infty} \sum_{q=-\infty}^{\infty} \delta(l - p\Delta\sigma, m - q\Delta\sigma). \tag{2.27}$$

The convolution with each of the delta functions in the reciprocal lattice will produce a shifted image of the original object as shown in Figure 2.10. If the object is small, then it is trivial to remove these 'ghost' images, but if it is greater than $\Delta\sigma$ in size then the ghost images overlap with the true image, and they become difficult or even impossible to disentangle from one another. Thus, good interferometric images can only be made of objects less than this size: the 'interferometric field of view' is therefore set by the density of sampling in the (u, v) plane. Other factors such as bandwidth smearing as discussed in Section 1.7 can also serve to restrict the field of view, but insufficient density of sampling is usually the most important factor that serves to limit the useful field of view.

2.4.4 Information efficiency

The results in the previous two subsections show that if the (u, v) plane is covered by a set of samples at a spacing of Δu and with maximum spacing $u_{\max}$

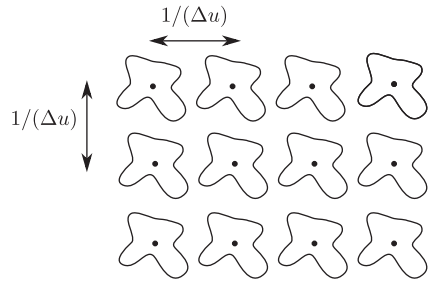

Figure 2.10 The lattice of reconstructed images caused by finite sampling.

then an image with angular resolution of about $1/(2u_{\max})$ radians and with a field of view of $1/(\Delta u)$ radians can be faithfully reconstructed. If $u = N \times \Delta u$ then the result could be represented as an image consisting of $2N \times 2N$ independent 'pixels' (these independent resolution elements are more correctly termed resels).

The samples used to make this image consist of an approximately $2N \times 2N$ grid in the (u, v) plane, and each fringe measurement yields two numbers, the real and imaginary parts of the coherent flux, so it might initially seem that twice as many numbers are measured as compared to the independent variables in the image. However, the Hermitian symmetry $F(\boldsymbol{u}) = F^*(-\boldsymbol{u})$ of the Fourier transform of a real object (see Section 2.2.6 and Appendix A) means that the measurements of coherent flux values in one half of the Fourier plane directly yield values for the opposite half. Hence only half of the number of measurements of the coherent flux need to be made as there are grid points, and so the 'information efficiency' of an appropriately sampled interferometric observation is almost exactly 100%, in the sense that the number of measurements equals the number of unknowns.

2.4.5 Wide-field interferometry

The above developments have assumed that the objects being observed are intrinsically small, specifically that they are smaller than the diffraction limit of a single collector, known as the 'primary beam' in radio interferometry. Radio interferometers can observe fields of view which are larger than the primary beam by using multiple pointings, and this is possible in principle at optical wavelengths. In practice, the possibility of observing such wide fields is restricted by a number of practical issues. The most fundamental of these is the requirement of dense (u, v)-plane sampling. In order to image a field of the

size of the diffraction limit of a collector of diameter D, i. e. a field of angular diameter $\theta = \lambda/D$, the baseline sampling required is of order $\Delta B \sim \lambda/\theta = D$; this means that the baseline spacing needs to be of the order of the telescope diameter. No current long-baseline interferometer has sufficient telescopes to approach this kind of baseline sampling and, as a result, wide-field-of-view imaging is not tackled in this book.